Origin of the Conformational Modulation of the (13)C NMR Chemical Shift of Methoxy Groups In Aromatic Natural Compounds.

ARTICLE *in* THE JOURNAL OF PHYSICAL CHEMISTRY A · JANUARY 2013

Impact Factor: 2.69 · DOI: 10.1021/jp310470f · Source: PubMed

4 AUTHORS, INCLUDING:

Michal Straka
Academy of Sciences of the Czech Republic
62 PUBLICATIONS **1,020** CITATIONS
SEE PROFILE

Vladimír Sklenář
Masaryk University
154 PUBLICATIONS **7,630** CITATIONS
SEE PROFILE

Radek Marek
Masaryk University
126 PUBLICATIONS **1,733** CITATIONS
SEE PROFILE

THE JOURNAL OF PHYSICAL CHEMISTRY A

Article

pubs.acs.org/JPCA

Origin of the Conformational Modulation of the ^{13}C NMR Chemical Shift of Methoxy Groups in Aromatic Natural Compounds

Jaromír Toušek,[†] Michal Straka,[†,‡] Vladimír Sklenář,[†,§,∥] and Radek Marek*[,†,§,∥]

[†]CEITEC - Central European Institute of Technology, Masaryk University, Kamenice 5/A4, CZ-62500 Brno, Czech Republic

[‡]Institute of Organic Chemistry and Biochemistry, Academy of Sciences of the Czech Republic, Flemingovo nám. 2, CZ-16610 Prague, Czech Republic

[§]National Center for Biomolecular Research, and [∥]Department of Chemistry, Faculty of Science, Masaryk University, Kamenice 5, CZ-62500 Brno, Czech Republic

Supporting Information

ABSTRACT: The interpretation of nuclear magnetic resonance (NMR) parameters is essential to understanding experimental observations at the molecular and supramolecular levels and to designing new and more efficient molecular probes. In many aromatic natural compounds, unusual ^{13}C NMR chemical shifts have been reported for out-of-plane methoxy groups bonded to the aromatic ring (~62 ppm as compared to the typical value of ~56 ppm for an aromatic methoxy group). Here, we analyzed this phenomenon for a series of aromatic natural compounds using Density Functional Theory (DFT) calculations. First, we checked the methodology used to optimize the structure and calculate the NMR chemical shifts in aromatic compounds. The conformational effects of the methoxy group on the ^{13}C NMR chemical shift then were interpreted by the Natural Bond Orbital (NBO) and Natural Chemical Shift (NCS) approaches, and by excitation analysis of the chemical shifts, breaking down the total nuclear shielding tensor into the contributions from the different occupied orbitals and their magnetic interactions with virtual orbitals. We discovered that the atypical ^{13}C NMR chemical shifts observed are not directly related to a different conjugation of the lone pair of electrons of the methoxy oxygen with the aromatic ring, as has been suggested. Our analysis indicates that rotation of the methoxy group induces changes in the virtual molecular orbital space, which, in turn, correlate with the predominant part of the contribution of the paramagnetic deshielding connected with the magnetic interactions of the $BD_{CMet-H} \rightarrow BD^*_{CMet-OMet}$ orbitals, resulting in the experimentally observed deshielding of the ^{13}C NMR resonance of the out-of-plane methoxy group.

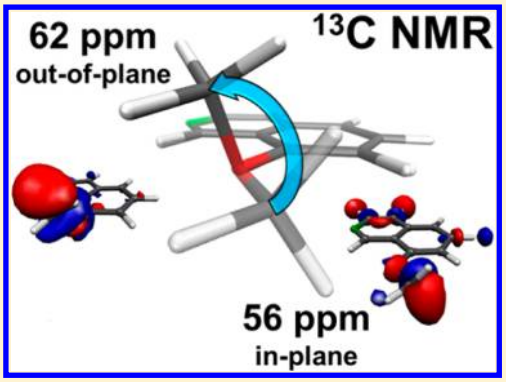

1. INTRODUCTION

NMR spectroscopy represents one of the most powerful techniques for characterizing the 3D molecular structure of chemical compounds both in solution and in the solid state.[1] Several observable NMR parameters can be used to probe a structure at the molecular and supramolecular levels. The NMR chemical shift of an individual atom, being very sensitive to its chemical and physical environment, is probably the most widely employed experimental NMR parameter. The isotropic chemical shifts, measured in solution or in the solid state, as well as the principal components of the chemical-shift tensors typically determined for solid samples, reflect the distribution of the electron density surrounding the nucleus of interest. The relative importance of individual physical effects (e.g., substitution, environment) on a particular chemical shift can be analyzed by quantum-chemical calculations.[2]

In this Article, we analyze and rationalize the structural effects on the NMR chemical shifts of the methoxy group for the four natural compounds listed in Scheme 1, specifically, the benzo[*c*]phenantridine alkaloids, 6-hydroxy-5,6-dihydrocheler-ythrine[3] (**1**) and norchelerythrine[4,5] (**2**), and the protoberber-ine alkaloids, 8-hydroxy-7,8-dihydropalmatine[6] (**3**) and tetrahy-droberrubine[7] (**4**). For convenience, the structures of norsanguinarine (**5**) and model compound **6** are also presented in this scheme.

Unusual ^{13}C NMR chemical shifts of ~62 ppm have been reported for the methoxy groups attached to aromatic carbons C7 (**1**), C7 (**2**), and C9 (**3**) in compounds **1**, **2**, and **3**, respectively. This chemical shift value is typically observed for molecules bearing bulky substituents in the neighborhood of the methoxy group in question. In the absence of a large substituent, the ^{13}C NMR chemical shift of the methyl carbon is ~56 ppm. This well-known effect[8−10] is related to the in-plane versus out-of-plane orientation of the methoxy group exhibiting different NMR chemical shifts and T_1 relaxation times.[11] Carter et al. investigated the ^{13}C NMR chemical shift tensors in methoxybenzenes and found an experimental difference of approximately 5 ppm for δ_{11} and 12 ppm for δ_{22}

Received: October 22, 2012
Revised: December 24, 2012
Published: December 26, 2012

Scheme 1. Structures and Atom Numbering Scheme for Compounds 1−6

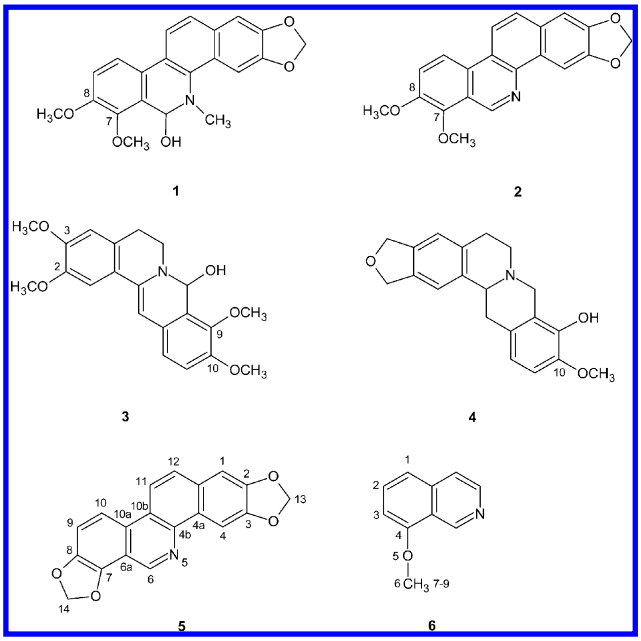

between the in-plane and out-of-plane orientations.[12] Further, using theoretical calculations, they identified significant deshielding contributed by the C−H bonds for the out-of-plane orientation of the methoxy group. Jardon et al.[13] suggested that in the absence of a neighboring substituent the methyl carbon is more shielded (∼56 ppm) because the in-plane orientation of the methoxy group enables better conjugation of the lone pair of electrons (LP) of the oxygen atom with the aromatic ring, whereas in the presence of two ortho substituents, the methoxy group is rotated out of the plane of the aromatic ring, and weaker conjugation of the oxygen LP with the aromatic system, accompanied by an accumulation of negative charge on the oxygen atom, is responsible for a reduced shielding of the methyl carbon (∼62 ppm). In contrast, Contreras et al.[14] have suggested that the increased electron conjugation should actually produce a deshielding effect on the carbon nucleus of the methoxy group. They offer an alternative explanation of this phenomenon based on the proximity of the methyl moiety to the aromatic ring.

In this Article, we aim at a full understanding and explanation of the unusual ^{13}C NMR chemical shifts of the methoxy group with respect to the electronic structure of the molecules studied. We employ Natural Bond Orbital (NBO),[15] Natural Chemical Shielding (NCS),[16] and excitation analyses[17] to further elucidate this phenomenon. The description provided by alternative localized orbital methods, such as bond conjugation and hyperconjugation, which originate from the delocalized features of the electronic structure, is complemented by NCS analysis, which uses direct calculations of nuclear shielding effects. Using NCS, nuclear magnetic shielding tensors computed by the Gauge-Including Atomic Orbital (GIAO)[18] method are partitioned into the magnetic contributions from the natural bond orbitals, which offer an intuitive explanation using the natural language of chemical bonds and lone pairs of electrons (LPs).

In the following, we demonstrate that the observed atypical ^{13}C NMR chemical shifts are not directly related to any different conjugation of the LP of the methoxy oxygen with the aromatic ring as has been suggested previously, but can be rationalized as reflecting the different orbital magnetic interactions between the occupied orbitals corresponding to the C−H bonds and the vacant antibonding C−O orbital, which shows the largest changes upon rotation of the methoxy group along the O−CH_3 axis.

2. COMPUTATIONAL METHODS

Gaussian 09 software[19] was used to optimize the molecular geometry at the DFT level and calculate the NMR shielding constants. The generalized gradient approximation (GGA) exchange-correlation DFT functionals BLYP,[20−22] and BP86,[23] as well as the hybrids B3LYP,[24−26] B3PW91,[27−31] PBE0 (also known as PBE1PBE),[32−34] and BHandHLYP,[35] were used in the calculations together with the basis sets 6-31G** (to optimize the geometry) and 6-311G** (to calculate the NMR shielding constants). The basis sets were selected on the basis of our previous experience.[5,36,37] The NMR shielding constants were calculated using the Gauge-Including Atomic Orbital (GIAO) method[17] to treat the gauge-dependence problem. Solvent effects were included using the polarizable continuum model (PCM) as implemented in the Gaussian 09 code.[38,39] The MAG-ReSpect[16] code at BP86/SVP level was used for the excitation analysis. The molecular orbitals were visualized using Molekel 4.3 software.[40] Excitation analysis breaks down the total nuclear magnetic shielding tensor for a particular atom into the contributions made by the different magnetic interactions between occupied and virtual orbitals. It is based on Ramsey's original formula.[41] Different input orbitals can be used in excitation analysis.[42−44] This work is based on Pipek−Mezey (PM)[45,46] localization of molecular orbitals in the framework of the Individual Localized Molecular Orbital (IGLO)[47] as well as their particular contributions to the nuclear shielding. Using excitation analysis, the contributions of PM localized molecular orbitals (PM-LMOs) to the magnetic shielding tensors can be divided into the individual magnetic interactions with the vacant molecular orbitals.

Natural chemical shielding (NCS) analysis as developed by Weinhold et al.[14,15] was used to break down the nuclear magnetic shielding tensors into the magnetic contributions from chemical bonds and LPs.

The calculated nuclear shieldings, σ(i), were converted into the corresponding chemical shifts, δ(i), using the shielding constant calculated for benzene as a secondary standard, σ(st). The reference molecule was calculated at the same level of theory as the molecules under study, and the chemical shifts were obtained as follows:

$$\delta(\mathrm{i}) = \sigma(\mathrm{st}) - \sigma(\mathrm{i}) + \delta(\mathrm{sec}) \quad (1)$$

where δ(sec) represents the experimental chemical shift of the secondary reference (benzene in benzene, ^{13}C = 127.8 ppm, ^{1}H = 7.16 ppm relative to TMS). The root-mean-square deviation between the calculated and experimental chemical shifts (RMSD) was calculated. Further, the RMSD^{rel} was calculated as the deviation between the correlated values and the line of best fit with the slope equal to 1. The RMSD shows how the selected method reproduces the absolute values of chemical shifts, whereas RMSD^{rel} shows how the method reproduces the differences between the experimental chemical shifts of the particular compound (trends in the NMR chemical shifts).

dx.doi.org/10.1021/jp310470f | J. Phys. Chem. A 2013, 117, 661−669

3. RESULTS AND DISCUSSION

To determine a reliable computational level that describes the nuclear magnetic shielding for compounds **1**−**4** with good accuracy, we tested several DFT functionals used for optimizing the molecular geometry and calculating the NMR shielding constants.[48−50] As our test compound, we selected the alkaloid norsanguinarine (compound **5**)[5] because it is a rigid molecule and calculations are not complicated by the existence of possible conformers.

3.1. Validation of DFT Methods Using Compound 5 (Norsanguinarine). *3.1.1. Effect of the Density Functional on the ^{13}C NMR Chemical Shifts for Compound 5.* We first investigated the influence of the density functional on the calculated ^{13}C NMR chemical shifts using B3PW91/6-31G** optimized geometry. The molecule was embedded in a PCM model using chloroform as the solvent. The best results for the ^{13}C NMR chemical shifts were obtained using the hybrid functionals B3LYP (RMSD^{rel}(^{13}C) = 0.9 ppm), B3PW91 (RMSD^{rel}(^{13}C) = 0.7 ppm), and PBE0 (RMSD^{rel}(^{13}C) = 0.7 ppm). The hybrid BHandHLYP (RMSD^{rel}(^{13}C) = 2.2 ppm) and the pure-DFT functionals BLYP (RMSD^{rel}(^{13}C) = 2.5 ppm) and BP86 (rsmd^{rel}(^{13}C) = 2.7 ppm) showed noticeably worse results (see also Tables S3 and S5, Supporting Information).

Because the results did not vary greatly with the correlation part of the functional (see the Supporting Information), we show a comparison of the experimental and calculated ^{13}C NMR chemical shifts only when the LYP correlation functional is combined with the three different exchange functionals, B, B3, and BHandH, with 0%, 20%, and 50% of exact-exchange admixture, respectively (Figure 1).

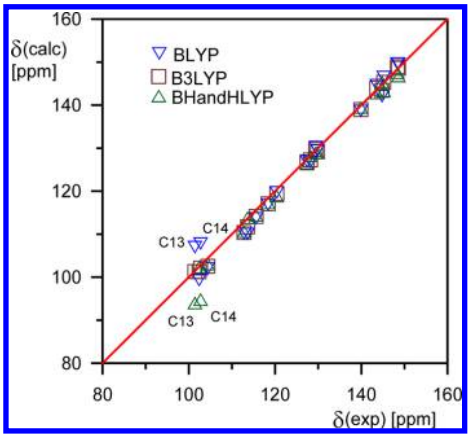

Figure 1. Experimental and DFT calculated ^{13}C NMR chemical shifts for the B3PW91/6-31G** optimized geometry of compound **5**.

The trends for the ^{13}C NMR chemical shifts of the aromatic carbons (Figure 1) were generally well reproduced. However, some noticeable discrepancies for the OCH_2O group (atoms C13 and C14) were evident. Whereas the B3LYP functional (and also B3PW91 and PBE0, as shown in Figure S1 in the Supporting Information) reproduced the NMR chemical shifts of the OCH_2O groups correctly, their values tended to be overestimated by the pure GGA functional BLYP (and by BP86, see Figure S3 in the Supporting Information) and underestimated by the hybrid GGA functional BHandHLYP with 50% of exact-exchange admixture. This is most probably attributable to the role of the electron correlation associated with the presence of the two LPs on each of two oxygen atoms bonded to each of the two carbon atoms C13 and C14.[51]

3.1.2. Effect of the Calculated Molecular Geometry on the NMR Chemical Shifts of Compound 5. To cross-validate the use of the B3PW91 geometry from section 3.1.1 and to check the influence of the optimized geometry on the NMR chemical shifts, we employed BLYP, B3LYP, B3PW91, and BHandHLYP geometries in combination with the B3PW91 chemical shift calculations. The results characterized by rsmd^{rel} were similar for all methods tested for the optimization of the structure with the exception of the BLYP functional (see Table S8, Supporting Information). Using the BLYP functional to optimize the geometry resulted in an overestimation of the ^{13}C NMR chemical shifts of the $-OCH_2O-$ groups (rsmd^{rel}(^{13}C) = 1.2 ppm). The most plausible explanation for this deviation can be found in the overestimation of the O−C13 (O−C14) bond lengths by ∼2 and ∼3 pm as compared to the experimental and the hybrid GGA geometry, respectively (see Table S1, Supporting Information).

On the basis of the results described in section 3.1, the B3PW91/6-31G** method was used to optimize the molecular geometries and the B3PW91/6-311G**(PCM) method for calculating the chemical shifts in production calculations. The results obtained for the ^{1}H NMR chemical shifts are summarized in Tables S4 and S7 (Supporting Information).

3.2. Conformational Dependence of the NMR Chemical Shift of Methoxy Group. The optimized B3PW91/6-31G** geometries of compounds **2** and **3** are shown in Figure 2 as examples to highlight the different orientations of the two types of methoxy groups in these systems. Note the one out-of-plane and one in-plane methoxy groups in **2** and one out-of-plane and three in-plane methoxy groups in **3**.

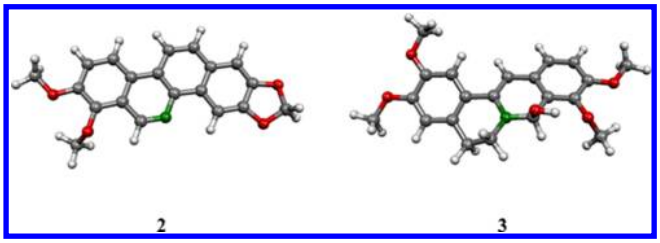

Figure 2. Molecular geometries of compounds **2** and **3** optimized by using B3PW91/6-31G** and highlighting the two different orientations of the two types of methoxy groups in these systems.

The ability of the selected protocol (B3PW91/6-311G**-(PCM)//B3PW91/6-31G**) to also reproduce the experimental differences between the ^{13}C NMR chemical shifts of the two different methoxy groups (as there is no $-OCH_3$ group in compound **5**, the selected test) was tested by means of calculations on compounds **1**−**4**. The experimentally measured and calculated ^{13}C chemical shifts are summarized in Table 1 together with the dihedral angles $C_{ar}-C_{ar}-O_{Met}-C_{Met}$ describing the orientations of the methoxy groups with respect to the aromatic ring. As is evident, the experimental differences are satisfactorily reproduced by the selected approach, and the ^{13}C NMR chemical shift of the $-OCH_3$ is systematically dependent on the orientation of the methoxy group. If the $O_{Met}-C_{Met}$ bond lies nearly in the plane of the aromatic ring ($C_{ar}-C_{ar}-O_{Met}-C_{Met} \approx 0°$), the experimental value of the C_{Met} chemical shift is approximately 56 ppm. If the $O_{Met}-C_{Met}$ bond is rotated out of the plane of the aromatic ring ($C_{ar}-C_{ar}-O_{Met}-C_{Met} \approx 70°$) because of steric interaction with a bulky

dx.doi.org/10.1021/jp310470f | J. Phys. Chem. A 2013, 117, 661−669

Table 1. Experimental and Calculated ^{13}C NMR Chemical Shifts δ [ppm] of the Methoxy Groups in 1−4 and the Orientations of These Methoxy Groups Relative to the Aromatic Ring[a]

	1			2			3			4		
atom	δ^{exp}	δ^{calc}	dih.	δ^{exp}	δ^{calc}	dih.	δ^{exp}	δ^{calc}	dih.	δ^{exp}	δ^{calc}	dih.
2-C_{Met}							56.4	49.9	0.1			
3-C_{Met}							56.2	50.1	−0.6			
7-C_{Met}	61.9	54.0	66.1	61.9	54.2	68.2						
8-C_{Met}	56.1	49.8	−2.4	56.9	50.1	−2.1						
9-C_{Met}							61.5	54.4	−68.7			
10-C_{Met}							56.6	49.7	1.5	55.9	50.2	−0.5

[a]Expressed as the dihedral angle $C_{ar}-C_{ar}-O_{Met}-C_{Met}$.

neighboring group, the value of the C_{Met} chemical shift is approximately 62 ppm. The corresponding calculated shifts are about 5 ppm smaller than the experimental values but retain the difference between the in-plane and out-of-plane orientations of the methoxy moiety. A better agreement of the computational data with the experimental values could be reached by using, for example, the chemical shift of the methoxy group of anisole as a secondary reference instead of benzene. This would, however, cause the results for the aromatic carbons to deteriorate. Accurate absolute numbers are not crucial for the analysis of the differences in the ^{13}C NMR chemical shift between the two orientations of the methoxy group.

To determine the reason for the 5−6 ppm difference between the ^{13}C NMR chemical shifts of the methoxy group in the in-plane and out-of-plane conformations, calculations were performed on a prototypic compound **6**. The aim was to find the extent to which the NMR chemical shift of the methyl carbon is influenced by the assumed conjugation of the LP of the O_{Met} with the aromatic moiety and how important are any roles played by other effects, such as steric interactions of the methyl group with other parts of the molecule, or hyperconjugation. The model compound **6** was chosen purposely to eliminate any possible further effects (e.g., electrostatic interaction of the methoxy group with a large ortho substituent).

The systematic dependence of the calculated ^{13}C NMR chemical shift of the methoxy group on the C3−C4−O5−C6 dihedral angle is shown in Figure 3 (see also Table S9 in the Supporting Information).

For a change in the dihedral angle from 0° (50.3 ppm) to 70° (58.8 ppm), a difference of ∼9 ppm is calculated, which is somewhat more than the difference of ∼5 ppm obtained for compounds **1**−**4**. The ^{13}C NMR chemical shifts for the in-plane methoxy groups in model compound **6** and compounds **1**−**4** ($\delta(C_{Met}) \approx 50$ ppm) are almost identical. Yet, a difference of about +5 ppm is obtained for the out-of-the-plane orientation of the methoxy group in model compound **6** ($\delta \approx 59$ ppm) as compared to compounds **1**−**4** ($\delta \approx 54$ ppm). This indicates that the bulky substituent positioned ortho to the out-of-plane methoxy group in compounds **1**−**4** significantly influences the ^{13}C NMR chemical shift of this methoxy group. This assumption was confirmed by calculating the chemical shift δ(C6) of the model compound with another methoxy group substituted at C3. The value of the calculated chemical shift was 54.0 ppm for C3−C4−O5−C6 = 70°, so the effect in the change of the orientation of the methoxy group with respect to the aromatic ring is even more than 5 ppm and is reduced by the presence of an ortho methoxy substituent. Although the ortho substituent reduces the difference between the NMR chemical shifts of the in-plane and out-of-plane orientations (probably by direct interaction with the methoxy group in question[52,53]), the trend is preserved, and further analysis of model compound **6** is therefore justified.

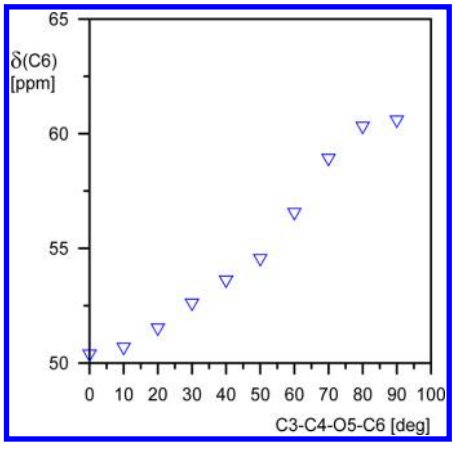

Figure 3. The dependence of the calculated chemical shift δ(C6) on the orientation of the methoxy group for model compound **6**.

3.3. Analysis of the Effects of Conjugation in Model Compound 6. The preference of the methoxy group for the in-plane conformation (e.g., 2-OMe, 3-OMe, and 10-OMe in compound **3**, Figure 2) points to the presence of a stabilizing interaction in the in-plane state.[11] Considering the role of the conjugative interaction of the LPs of oxygen (O5) with the neighboring aromatic system, two principal questions will be addressed.

First, how much does the conjugative interaction vary during the rotation of the methoxy group (cf., Figure 3)? NBO analysis was done for the two extreme orientations of the methoxy group: in-plane (C3−C4−O5−C6 = 0°) and out-of-plane (C3−C4−O5−C6 = 90°). There are two LPs located on the oxygen atom, denoted as LP^{π}_{O5} and LP^{σ}_{O5} (only LP^{π}_{O5} is shown in Figure 4a). A strong interaction, characterized by an

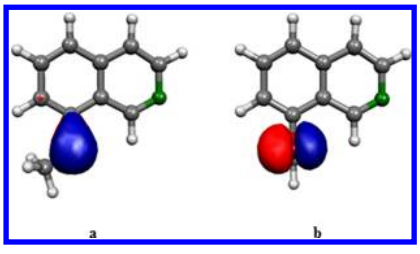

Figure 4. NLMO orbital LP^{π}_{O5} calculated for the two extreme orientations of the methoxy group.

dx.doi.org/10.1021/jp310470f | J. Phys. Chem. A 2013, 117, 661−669

energy level of −33.7 kcal mol^{-1}, of the LP$^{\pi}_{O5}$ with the antibonding orbital C3−C4 of the aromatic ring (BD*$_{C3-C4}$)[54] occurs for the in-plane orientation of the methoxy group. It decreases significantly for the out-of-plane orientation (−6.6 kcal mol^{-1}). In other words, the stabilizing conjugation of the LP$^{\pi}_{O5}$ with the aromatic ring is greatest for the in-plane orientation of the methoxy group (Figure 4a) and is significantly less for the out-of-plane conformation (Figure 4b).

Second, is there any direct relation between the LP$^{\pi}_{O5}$→BD*$_{C3-C4}$ stabilizing interaction and the NMR chemical shifts of the atoms in the system? The natural chemical shielding (NCS) analysis shown in Table 2 reveals that the shielding

Table 2. Nuclear Magnetic Shielding Constants σ (ppm) and Direct Contributions of the Lone Pair of Electrons on O5 Atom (LP$^{\pi}_{O5}$) to σ in 6 Obtained from NCS Analysis

	C3−C4−O5−C6			
	0°		90°	
atom	total	LP$^{\pi}_{O5}$	total	LP$^{\pi}_{O5}$
C3	80.8	0.0	62.9	−3.4
C4	24.9	−0.7	21.7	2.1
C6	131.5	1.5	121.3	0.4
O5	228.7	3.3	266.1	−25.4

constant of O5 is strongly influenced by the orientation-dependent contribution of LP$_{O5}$, which correlates with the previous experimental and theoretical results.[55] The shielding constants of C3 and C4 are modulated moderately by the contribution of LP$_{O5}$, and, a bit surprisingly, the contribution of LP$_{O5}$ to σ_{C6} is almost conformation invariant. Hence, we observe no direct connection between the delocalization of the LP of the oxygen atom and the shielding at the methoxy carbon upon the rotation of the methoxy group.

To investigate the conformational profile in more detail, the dependence of the relative contributions of the most important NLMOs to the ^{13}C NMR chemical shift of the C6 atom on the molecular geometry (specifically the dihedral angle C3−C4−O5−C6) was evaluated by using NCS analysis. The results are shown in Figure 5. The most important conformation-dependent contributions arise from the C6−O5 bond and from the three C6−H bonds (Figure 5). The contributions from the LPs of the O5 atom are marginal (Figure 5). The correlation coefficients of the $\Sigma\sigma_{C6-H}$, σ_{C6-O5}, and ΣLP$_{O5}$ contributions with δ_{C6} were calculated (Figures S6−S8 in the Supporting Information). These data show that the dependence of δ_{C6} on the dihedral angle C3−C4−O5−C6 correlates well with the sum of the contributions of the three C6−H bonds (R^2 = 0.97).

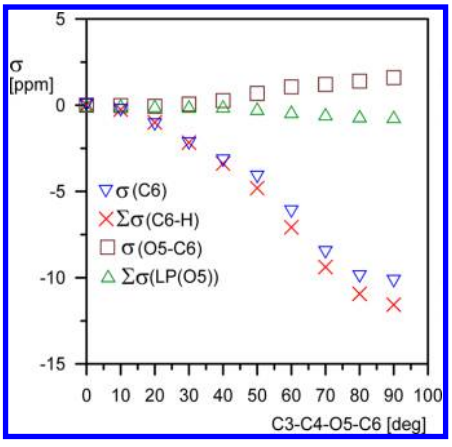

Figure 5. The conformational dependence of the NCS contributions of selected NLMOs (ΣBD$_{C6-H}$, BD$_{O5-C6}$, and ΣLP$_{O5}$) to the chemical shift δ_{C6} on the orientation of the methoxy group in compound **6**. The total nuclear magnetic shielding and NLMO contributions are scaled to 0 ppm for the in-plane orientation (C3−C4−O5−C6 = 0°) for better clarity.

The NCS contributions of the C6−H bonds can be further divided into diamagnetic and paramagnetic parts. The difference in the paramagnetic contributions between the in-plane and out-of-plane orientations of the methoxy group is −13.38 ppm. Comparison with the total difference (−11.57 ppm) provides evidence that the difference in the chemical shift of C6 is controlled mainly by the paramagnetic contribution, while the changes in the diamagnetic part, opposite to the observed trend, only slightly reduce its magnitude.

Interestingly, while the NCS analysis shows the $\Sigma\sigma_{C6-H}$ contributions to be the main source of the conformational dependence of the ^{13}C NMR chemical shift of the methoxy group, the NLMOs corresponding to the C−H bonds do not appear to change at all upon rotation of the methoxy group (numbers not shown). Hence, the excitation analysis described in the following sections has been employed.

3.4. Excitation Analysis of the ^{13}C NMR Chemical Shift Tensor of −OMe Group in Compound 6. In Ramsey's theory,[41] the nonrelativistic nuclear magnetic shielding tensor of nucleus K is expressed as the sum of the diamagnetic (d) and paramagnetic (p) components:

$$\sigma_K = \sigma_K^{d} + \sigma_K^{p} \tag{2}$$

The paramagnetic part, which is principally responsible for the chemical shift, can be expanded into a sum-over-states of orbital contributions as follows:

$$\sigma_K^{p} = \alpha^2 \sum_{i}^{occ} \sum_{a}^{virt} \frac{\langle i|\mathbf{l}_{iO}|a\rangle\langle a|\mathbf{l}_{iK}/r_{iK}^3|\rangle}{e_i - e_a} + \text{cc} \tag{3}$$

where α is a fine structure constant. The two integrals represent the orbital Zeeman (OZ) interaction and the paramagnetic nuclear spin−electron orbit (PSO) interaction, while the denominators correspond to the energy differences between the virtual (a) and occupied (i) orbitals.

According to eq 3, used in excitation analysis, the paramagnetic component of the magnetic shielding tensor arises from interactions between the occupied and unoccupied molecular orbitals. The contribution of the particular interaction increases (in absolute value) with the decreasing difference in energy between the two orbitals in the denominator and increasing values of the OZ and PSO terms. The latter change requires that the angular momentum operator transforms an occupied MO into a form that overlaps well with the appropriate unoccupied MO. This corresponds to a paramagnetic ring current in the plane containing the two MOs involved and a corresponding major contribution to the σ^{p} points perpendicular to this plane. In other words, the preferred magnetic rotation around an axis leads to large σ^{p} contributions along this axis.[42−44]

The application of Ramsey's equation is demonstrated here on the interactions of BD$_{C6-H7}$ (the orientation of the C6−H7 bond is characterized by the dihedral angle C4−O5−C6−H7 = 180°) for the in-plane orientation of the methoxy group. The

dx.doi.org/10.1021/jp310470f | J. Phys. Chem. A 2013, 117, 661−669

Table 3. Contributions of the Methoxy C6−H Orbital Interactions with the Selected Vacant Molecular Orbitals MO_{48} and MO_{53} to the Particular Components of the C6 Shielding Tensor (ppm), the Corresponding Energy Denominators (eV), and OZ (mHartree/Zeeman), as well as PSO (mZeeman) Matrix Elements for the In-Plane Orientation of the Methoxy Group

PM-LMO		MO	σ_{xx}	σ_{yy}	σ_{zz}	E	OZ	PSO
C6−H7	→	48	0.0	**−13.9**	**0.0**	−9.6	0.5	2.5
C6−H8	→	48	−15.5	−3.4	0.0	−18.9	1.2	2.7
C6−H9	→	48	−12.9	−4.9	0.0	−10.4	0.7	2.7
C6−H7	→	53	−2.8	**0.0**	**−13.2**	−11.0	0.4	4.7
C6−H8	→	53	0.5	0.0	−3.6	−20.2	0.3	2.7
C6−H9	→	53	0.1	0.0	−5.2	−11.8	0.2	2.8

contributions of the magnetic interactions of the localized C6−H orbital with the selected vacant canonical molecular orbitals to the individual components of the C6 shielding tensor, with the corresponding energy denominators as well as the OZ and PSO terms, are summarized in Table 3.

We selected two interactions as examples to demonstrate the conclusions that can be drawn from the results of the excitation analysis presented in Table 3. The $BD_{C6-H7}\rightarrow MO_{48}$ orbital interaction produces a significant contribution to the σ_{yy} component of C6 shielding tensor (−13.9 ppm, as shown in bold in Table 3), while the contributions of this excitation to σ_{xx} and σ_{zz} are negligible. BD_{C6-H7} and MO_{48} for the in-plane orientation of the methoxy group (Figure 6) are shown from

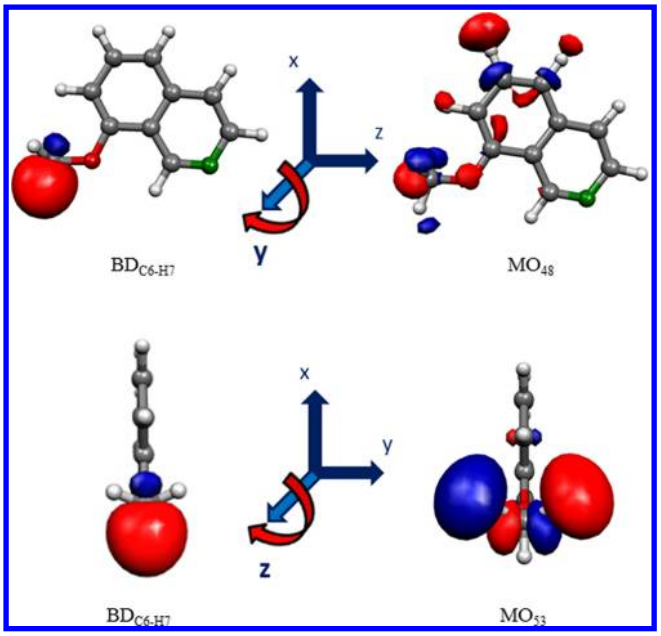

Figure 6. Schematic representation of the $BD_{C6-H7}\rightarrow MO_{48}$ orbital magnetic interaction producing a significant contribution to the σ_{yy} component of the C6 shielding tensor (−13.9 ppm) and the $BD_{C6-H7}\rightarrow MO_{53}$ orbital magnetic interaction producing a significant contribution to the σ_{zz} component of the C6 shielding tensor (−13.2 ppm).

the y direction of the C6 shielding tensor; the origin of the coordinate system is located at the position of atom C6. It is clear from Figure 6 that the rotation of the C6−H7 bonding LMO around the y principal axis produces a transformed MO that overlaps nicely with the vacant MO_{48} at the location of the C6 atom, resulting in a significant contribution to the σ_{yy} component of the C6 shielding tensor. On the contrary, rotation of BD_{C6-H7} around the x or z principal axis does not lead to its overlap with MO_{48}, and therefore the contributions of this magnetic interaction to σ_{xx} and σ_{zz} are negligible (Table 3).

The contrasting example, bearing totally different consequences for the orientation, is represented by the $BD_{C6-H7}\rightarrow MO_{53}$ interaction. In this case, there is a significant contribution to the σ_{zz} component of the C6 shielding tensor (−13.2 ppm, see Table 3), whereas the contributions to the σ_{xx} and σ_{yy} components are small or negligible. The origin of this behavior becomes clear when analyzing the interaction schematically visualized in Figure 6, where both the BD_{C6-H7} and the vacant MO_{53} are viewed from the z principal axis of the C6 shielding tensor. In this case, the rotation of the BD_{C6-H7} produces a transformed MO that overlaps with MO_{53}, while rotations around the x or y principal axis do not lead to favorable interaction.

Because the experimental NMR data are measured in isotropic solutions, the fast rotation of methyl group around the O−CH_3 bond results in the summing of the contributions of all three C−H bonds. The contributions of the sums of the C6−H orbital interactions with the selected vacant molecular orbitals to the σ_{xx}, σ_{yy}, and σ_{zz} components of the C6 shielding tensor for the two extreme orientations of the methoxy group are summarized in Table 4. The trends revealed by the above-demonstrated individual C−H bonds are preserved after averaging (compare the two examples in Tables 3 and 4 highlighted in bold).

Table 4. Contributions of the Sums of the C6−H Interactions to the σ_{xx}, σ_{yy}, and σ_{zz} Components of the C6 NMR Shielding Tensor (ppm) in Compound 6

	C2−C5−O11−C15 = 0°			C2−C5−O11−C15 = 90°		
MO	σ_{xx}	σ_{yy}	σ_{zz}	σ_{xx}	σ_{yy}	σ_{zz}
43	0.0	0.0	0.0	−10.5	−3.2	0.2
47	0.0	0.0	0.0	−10.7	−8.3	−1.6
48	−28.4	**−22.2**	**0.1**	−25.6	−24.8	0.0
49	−16.3	−15.7	−0.3	−2.1	−4.3	0.1
50	−13.6	−12.3	−1.1	−30.1	−31.7	0.0
53	−2.3	**0.0**	**−22.0**	−1.8	0.0	−9.2

Further, because we are dealing with isotropic ^{13}C NMR chemical shifts in solution, the contributions of the MO to the individual tensor components must be averaged, as analyzed and rationalized in section 3.5.

3.5. Rationalizing the Conformational Modulation of the ^{13}C NMR Chemical Shift of the −OMe Group in Compound 6. The contributions of the sums of the C6−H interactions with the selected vacant molecular orbitals and the sums of the interactions with all of the vacant CMOs to the isotropic ^{13}C NMR chemical shift of the C6 atom for the two

dx.doi.org/10.1021/jp310470f | J. Phys. Chem. A 2013, 117, 661−669

extreme orientations of the methoxy group are summarized in Table 5.

Table 5. Contributions of the C6−H Orbital Interactions (ΣBD_{C6-H}) with Selected Virtual MOs to the NMR Shielding Constant (ppm) of C6 in Compound 6

MO	C3−C4−O5−C6 = 0°	C3−C4−O5−C6 = 90°	Δ
43	0.0	−4.5	−4.5
47	0.0	−6.7	−6.7
48	−16.9	−16.8	+0.1
49	−10.6	−2.3	+8.3
50	−9.0	−20.7	−11.7
53	−10.2	−3.6	+6.6
Σ	−46.7	−54.6	**−7.9**
total	−93.7	−103.2	−9.5

The most significant difference between the in-plane (0°) and out-of-plane (90°) conformation is observed for the deshielding contribution of $\Sigma BD_{C6-H} \rightarrow MO_{50}$, which increases for the out-of-plane orientation of the methoxy group. The values of the particular $BD_{C6-H} \rightarrow MO_{50}$ contributions (−9.0 ppm vs −20.7 ppm) may be rationalized in a similar way as demonstrated in section 3.4. For example, the $BD_{C6-H7} \rightarrow MO_{50}$ contribution for the in-plane orientation characterized by $(OZ \cdot PSO)/\Delta E = (0.3 \cdot 1.6)/-10.4 = -0.05$ induces deshielding of −5.6 ppm in the σ_{yy} component (see Table 6). The difference in energy for the same excitation in the out-of-plane conformation is somewhat larger (−13.9 eV). However, the increased OZ and PSO terms outweigh the increase in the energy gap, and the total $(OZ \cdot PSO)/\Delta E = (1.0 \cdot 2.3)/-13.9 = -0.16$ is responsible for an increased deshielding contribution of −16.6 ppm to the σ_{yy} component. The difference in the corresponding orbital interactions between the two extreme orientations of the methoxy group can be attributed to the different spatial properties of the virtual MO_{50} shown in Figure 7. MO_{50} is less localized in the area of the C6 atom for the in-plane orientation (16.1% of the C6 AOs) as compared to the out-of-plane orientation (33.2%). This difference results in a more efficient overlap and a larger deshielding contribution to the C6 NMR shielding tensor for the out-of-plane conformation.

To highlight the importance of the $BD_{C6-H} \rightarrow MO_{50}$ interactions, we calculated the sum of the contributions of all of the C6−H bonds (see Table 6). The difference between the in-plane and out-of-plane conformations amounts, for the individual principal components, to approximately −16 ppm for σ_{xx} and −19 ppm for σ_{yy}, whereas the difference for σ_{zz} is marginal. These differences correlate with the experimental trend reported for the methoxybenzenes: $\Delta\delta_{11} \approx -5$ ppm, $\Delta\delta_{22} \approx -12$ ppm, and $\Delta\delta_{33} \approx 0$ ppm.[12]

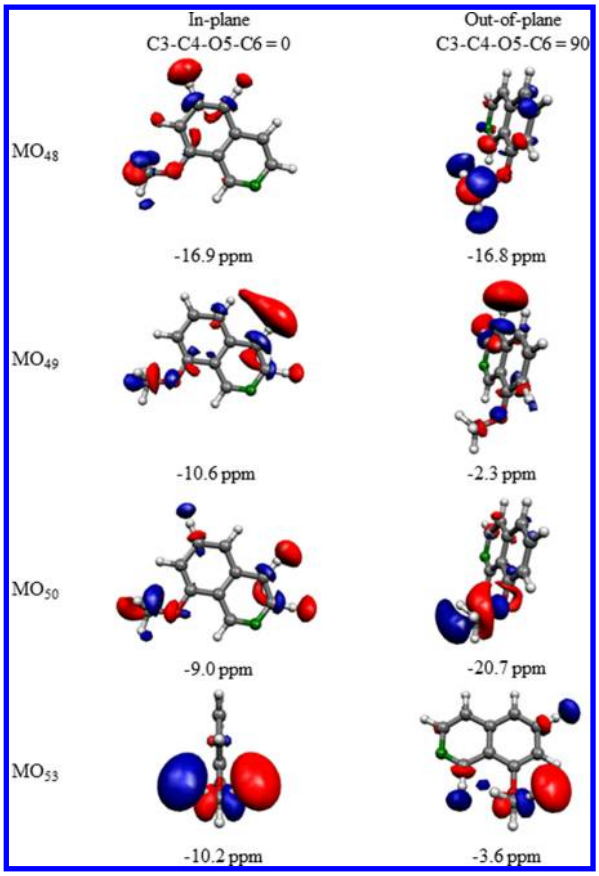

Figure 7. Visualization of selected MOs calculated for the two extreme orientations of the methoxy group and the corresponding sums of the contributions of the C6−H interactions with virtual MO to the NMR shielding constant of C6 in compound **6**.

The $\Sigma BD_{C6-H} \rightarrow MO_{49}$ contribution to the deshielding also depends significantly on the conformation of the methoxy group, with a smaller contribution for the out-of-plane orientation. This effect is the opposite of that calculated for the $\Sigma BD_{C6-H} \rightarrow MO_{50}$ orbital interaction. In contrast to the case involving MO_{50}, the contribution of the C6 atomic orbitals to the vacant MO_{49} decreases for the out-of-plane orientation of the methoxy group (6.7% for the out-of-plane orientation vs 9.6% for the in-plane). As a result, the OZ and PSO terms decrease, reducing the paramagnetic contribution to the deshielding (Table S10). The contribution of the $\Sigma BD_{C6-H} \rightarrow MO_{48}$ interaction is almost independent of the conformation, and the difference between the in-plane and out-of-plane contributions therefore amounts to only 0.1 ppm (see Table 5). The contribution of the $BD_{C6-H7} \rightarrow MO_{53}$ interaction has already been demonstrated for the in-plane orientation in

Table 6. Contributions of the Methoxy C6−H Orbital Interactions with a Vacant MO_{50} Molecular Orbital to Particular Components of the C6 Shielding Tensor (ppm), the Corresponding Energy Denominators (eV), and the OZ [mHartree/Zeeman] and PSO [mZeeman] Matrix Elements for the Two Extreme Orientations of the Methoxy Group

	C2−C5−O11−C15 = 0°						C2−C5−O11−C15 = 90°					
PM-LMO	σ_{xx}	σ_{yy}	σ_{zz}	E	OZ	PSO	σ_{xx}	σ_{yy}	σ_{zz}	E	OZ	PSO
C6−H7	0.0	−5.6	0.0	−10.4	0.3	1.6	−1.0	−16.6	0.1	−13.9	1.0	2.3
C6−H8	−7.7	−2.9	−0.7	−19.7	0.8	2.6	−18.9	−3.0	0.0	−13.1	1.0	2.7
C6−H9	−5.9	−3.8	−0.5	−11.3	0.4	2.6	−10.2	−12.2	−0.1	−14.3	1.1	2.8
Σ	−13.6	−12.3	−1.2				−30.1	−31.8	0.0			

dx.doi.org/10.1021/jp310470f | J. Phys. Chem. A 2013, 117, 661−669

Figure 6. Because the contributions of the C6 AOs to MO_{53} are smaller for the out-of-plane orientation of the methoxy group (7.3% for the out-of-plane vs 22.9% for the in-plane), the corresponding contribution to the deshielding is reduced from −10.2 to −3.6 ppm (Table 5).

Two significant contributions come from the $\Sigma BD_{C6-H} \rightarrow MO_{43}$ and $\Sigma BD_{C6-H} \rightarrow MO_{47}$ interactions, both of which contribute non-negligibly only to the out-of-plane conformation. For example, whereas the C6 AOs contribute 17.0% to MO_{47}, the same contributions are vanishingly small for the in-plane orientation (0.1%). MO_{43} and MO_{47} are shown for both orientations in the Supporting Information (Figure S9 and Tables S10 and S11).

Summing, the contributions of the six selected orbital interactions summarized in Table 5 shows a difference of approximately −8 ppm between the in-plane and out-of-plane conformations, which correlates nicely with the total difference $\Delta\sigma \approx -9$ ppm. Clearly, these six interactions represent the overwhelming majority of the conformation-dependent contributions to the ^{13}C NMR chemical shift of the methoxy group.

In summary, the conformational modulation of the C6 NMR chemical shift cannot be explained by a single effect. In general, this modulation originates in changes in the shapes of several virtual MOs. The most significant difference is observed for the canonical MO_{50}, which corresponds to the antibonding BD^*_{O5-C6}. Therefore, the interactions of the three C6−H bonding orbitals with the O5−C6 virtual antibonding orbital, which exhibit different spatial properties for the two different extreme conformations of the methoxy group (being more delocalized for the in-plane conformation), are mainly responsible for the conformational modulation of the ^{13}C NMR chemical shift of the methoxy group.

3.6. Generalization for Compounds 1−4. To generalize the findings described above, the sums of the contributions of the C_{Met}−H bonds to the ^{13}C NMR shielding constants of the methyl groups were calculated for the equilibrium geometries of compounds **1**−**4** (Table 7). The differences between the sums of the contributions for the in-plane and out-of-plane orientations of the methoxy group correspond nicely to the values obtained for the model system **6** (Table S12, Supporting Information), indicating that the conclusions formulated above for model compound **6** can also be applied for compounds **1**−**4** and are generally valid for any aromatic system bearing a methoxy group.

Table 7. Contributions of $\Sigma\sigma_{CMet-H}$ to the ^{13}C NMR Shielding Constants (ppm) of the Methoxy Groups in Compounds 1−4 Obtained by NCS Analysis

	$\Sigma\sigma_{CMet-H}$			
atom	1	2	3	4
2-C_{Met}			−54.4	
3-C_{Met}			−48.1	
7-C_{Met}	−55.1	−55.5		
8-C_{Met}	−46.7	−47.1		
9-C_{Met}			−54.7	
10-C_{Met}			−46.3	−44.9

4. CONCLUSIONS

The conformational dependence of the ^{13}C NMR chemical shift of methoxy groups in aromatic compounds was analyzed using Density Functional Theory. Several DFT functionals for optimizing the molecular geometry and calculating the NMR chemical shifts were tested for the reference compound norsanguinarine (**5**), a benzo[*c*]phenantridine alkaloid derivative. The best results were obtained by using three hybrid GGA functionals with 20−25% of exact-exchange admixture, B3PW91, B3LYP, and PBE0. B3PW91 was applied for calculations of the studied compounds (**1**−**4**).

NBO, NCS, and excitation analyses were used to investigate the effects of the conformation and the electronic structure on the ^{13}C NMR chemical shift of the methoxy group. It was confirmed that the conjugation of the LP on the oxygen atom with the aromatic ring is modulated by the conformation of the methoxy group. However, this conjugation interaction does not directly affect the ^{13}C NMR chemical shift of the methoxy group. According to the results obtained from the NCS analysis, the paramagnetic contributions of the C_{Met}−H bonds are mainly responsible for the conformational modulation of the ^{13}C NMR chemical shift of the methoxy groups. The contributions of the C_{Met}−H bonds were further studied via excitation analysis using Ramsey's formula, which allows breaking the NMR shielding constant into the individual contributions in terms of the orbital magnetic interactions of the occupied and virtual MOs. The modulation of the ^{13}C NMR chemical shift upon rotation of the methoxy group originates in changes in the shapes of several virtual MOs. The most significant conformational dependence is observed for the virtual MO that corresponds to the O_{Met}−C_{Met} antibonding MO, which undergoes large changes in shape and distribution upon rotation of the methyl group (being more delocalized for the in-plane orientation).

In summary, the interactions of the C_{Met}−H bonding orbitals with the O_{Met}−C_{Met} antibonding orbital, characterized by conformation-dependent delocalization, are mainly responsible for the modulation of the ^{13}C NMR chemical shift of the −OMe group. We have shown with a series of compounds that the conclusions drawn in this article are generally valid for any aromatic system bearing a methoxy group.

■ ASSOCIATED CONTENT

Supporting Information

Tables S1 and S2 with calculated structural parameters for norsanguinarine, S3−S8 with calculated NMR chemical shifts and RMSD's for norsanguinarine, S9 with the geometrical dependence of the NMR chemical shifts and the NCS contributions for **6**, S10 and S11 with the results of the excitation analysis, Figures S1−S5 with comparisons of the experimental and calculated chemical shifts of norsaguinarine, S6−S8 with the results of the NCS analysis and the correlation coefficients, S9 with selected MOs, and the atomic coordinates for the optimized geometries of compounds **1**−**5**. This material is available free of charge via the Internet at http://pubs.acs.org.

■ AUTHOR INFORMATION

Corresponding Author

*E-mail: rmarek@chemi.muni.cz.

Notes

The authors declare no competing financial interest.

■ ACKNOWLEDGMENTS

This work was supported by the project "CEITEC − Central European Institute of Technology" (CZ.1.05/1.1.00/02.0068)

from the European Regional Development Fund. M.S. was supported by the Czech Academy of Sciences (RVO 61388963). The access to computing and storage facilities owned by parties and projects contributing to the National Grid Infrastructure MetaCentrum, and provided under the program "Projects of Large Infrastructure for Research, Development, and Innovations" (LM2010005) and the CERIT-SC computing and storage facilities provided under the program Center CERIT Scientific Cloud, part of the Operational Program Research and Development for Innovations, reg. no. CZ. 1.05/3.2.00/08.0144, is acknowledged.

REFERENCES

(1) Croasmun, W. R., Carlson, R. M. K., Eds. *Two-Dimensional NMR Spectroscopy*; VCH: New York, 1994; pp 619−914.
(2) Kaupp, M., Bühl, M., Malkin, V. G., Eds. *Calculation of NMR and EPR Parameters. Theory and Application*; Wiley-VCH: Weinheim, Germany, 2004; pp 153−277.
(3) Toušek, J.; Dommisse, R.; Dostál, J.; Žák, Z.; Pieters, L.; Marek, R. *J. Mol. Struct.* **2002**, *613*, 103−113.
(4) Marek, R.; Marek, J.; Dostál, J.; Táborská, E.; Slavík, J.; Dommisse, R. *Magn. Reson. Chem.* **2002**, *40*, 687−692.
(5) Toušek, J.; Dostál, J.; Marek, R. *J. Mol. Struct.* **2004**, *689*, 115−120.
(6) Marek, R.; Sečkářová, P.; Hulová, D.; Marek, J.; Dostál, J.; Sklenář, V. *J. Nat. Prod.* **2003**, *66*, 481−486.
(7) Chudík, S.; Marek, R.; Sečkářová, P.; Nečas, M.; Dostál, J.; Slavík, J. *J. Nat. Prod.* **2006**, *69*, 954−956.
(8) Kan-Fan, Ch.; Massiot, G.; Das, B. C.; Potier, P. *J. Org. Chem.* **1981**, *46*, 1481−1483.
(9) Makriyannis, A.; Knittel, J. J. *Tetrahedron Lett.* **1979**, *20*, 2753−2756.
(10) Schuster, I. I. *J. Org. Chem.* **1985**, *50*, 1656−1662.
(11) Makriyannis, A.; Fesik, S. *J. Am. Chem. Soc.* **1982**, *104*, 6462−6463.
(12) Carter, C. M.; Facelli, J. C.; Alderman, D. V.; Grant, D. M.; Dalley, N. K.; Wilson, B. E. *J. Chem. Soc., Faraday Trans. 1* **1988**, *84*, 3673−3690.
(13) Jardon, P. W.; Vickery, E. H.; Pahler, L. F.; Pourahmady, N.; Mains, G. J; Eisenbraun, E. J. *J. Org. Chem.* **1984**, *49*, 2130−2135.
(14) Contreras, R. H.; Biekofsky, R. B.; de Kowalewski, D. G.; Orendt, A. M.; Facelli, J. C. *J. Phys. Chem.* **1993**, *97*, 91−93.
(15) Glendening, E. D.; Reed, A. E.; Carpenter, J. E.; Weinhold, F. *NBO Version 3.1*.
(16) Bohmann, J. A.; Weinhold, F.; Farrar, T. C. *J. Chem. Phys.* **1997**, *97*, 1173−1184.
(17) Malkin, V. G.; Malkina, O. L.; Reviakine, R.; Arbuznikov, A. V.; Kaupp, M.; Schimmelpfennig, B.; Malkin, I.; Helgaker, T.; Ruud, K. *MAG-Respect, version 1.1*, 2003.
(18) Wolinski, K.; Hilton, J. F.; Pulay, P. *J. Am. Chem. Soc.* **1990**, *112*, 8251−8260.
(19) Frisch, M. J.; Trucks, G. W.; Schlegel, H. B.; Scuseria, G. E.; Robb, M. A.; Cheeseman, J. R.; Scalmani, G.; Barone, V.; Mennucci, B.; Petersson, G. A.; Nakatsuji, H.; Caricato, M.; Li, X.; Hratchian, H. P.; Izmaylov, A. F.; Bloino, J.; Zheng, G.; Sonnenberg, J. L.; Hada, M.; Ehara, M.; Toyota, K.; Fukuda, R.; Hasegawa, J.; Ishida, M.; Nakajima, T.; Honda, Y.; Kitao, O.; Nakai, H.; Vreven, T.; Montgomery, J. A., Jr.; Peralta, J. E.; Ogliaro, F.; Bearpark, M.; Heyd, J. J.; Brothers, E.; Kudin, K. N.; Staroverov, V. N.; Kobayashi, R.; Normand, J.; Raghavachari, K.; Rendell, A.; Burant, J. C.; Iyengar, S. S.; Tomasi, J.; Cossi, M.; Rega, N.; Millam, J. M.; Klene, M.; Knox, J. E.; Cross, J. B.; Bakken, V.; Adamo, C.; Jaramillo, J.; Gomperts, R.; Stratmann, R. E.; Yazyev, O.; Austin, A. J.; Cammi, R.; Pomelli, C.; Ochterski, J. W.; Martin, R. L.; Morokuma, K.; Zakrzewski, V. G.; Voth, G. A.; Salvador, P.; Dannenberg, J. J.; Dapprich, S.; Daniels, A. D.; Farkas, Ö.; Foresman, J. B.; Ortiz, J. V.; Cioslowski, J.; Fox, D. J. *Gaussian 09*, revision A.1; Gaussian, Inc.: Wallingford, CT, 2009.
(20) Becke, A. D. *Phys. Rev. A* **1988**, *38*, 3098−30100.
(21) Lee, C.; Yang, W.; Parr, R. G. *Phys. Rev. B* **1988**, *37*, 785−789.
(22) Miehlich, B.; Savin, A.; Stoll, H.; Preuss, H. *Chem. Phys. Lett.* **1989**, *157*, 200−206.
(23) Perdew, J. P. *Phys. Rev. B* **1986**, *33*, 8822−8824.
(24) Becke, A. D. *J. Chem. Phys.* **1993**, *98*, 5648−5652.
(25) Vosko, S. H.; Wilk, L.; Nusair, M. *Can. J. Phys.* **1980**, *58*, 1200−1211.
(26) Stephens, P. J.; Devlin, F. J.; Chabalovski, C. F.; Frisch, M. J. *J. Phys. Chem.* **1994**, *98*, 11623−11627.
(27) Perdew, J. P. In *Electronic Structure of Solids '91*; Ziesche, P., Eschrig, H., Eds.; Akademie Verlag: Berlin, 1991; p 11.
(28) Perdew, J. P.; Chevary, J. A.; Vosko, S. H.; Jackson, K. A.; Pederson, M. R.; Singh, D. J.; Fiolhais, C. *Phys. Rev. B* **1992**, *46*, 6671−6687.
(29) Perdew, J. P.; Chevary, J. A.; Vosko, S. H.; Jackson, K. A.; Pederson, M. R.; Singh, D. J.; Fiolhais, C. *Phys. Rev. B* **1993**, *48*, 4978.
(30) Perdew, J. P.; Burke, K.; Wang, Y. *Phys. Rev. B* **1996**, *54*, 16533−16539.
(31) Perdew, J. P.; Burke, K.; Wang, Y. In *Electronic Density Functional Theory: Recent Progress and New Directions*; Dobson, J. F., Vignale, G., Das, M. P., Eds.; Plenum: New York, 1998.
(32) Perdew, J. P.; Burke, K.; Ernzerhof, M. *Phys. Rev. Lett.* **1996**, *77*, 3865−3868.
(33) Perdew, J. P.; Burke, K.; Ernzerhof, M. *Phys. Rev. Lett.* **1997**, *78*, 1396.
(34) Adamo, C.; Barone, V. *J. Chem. Phys.* **1999**, *110*, 6158−6169.
(35) Becke, A. D. *J. Chem. Phys.* **1993**, *98*, 1372−1377.
(36) Maliňáková, K.; Novosadová, L.; Lahtinen, M.; Kolehmainen, E.; Brus, J.; Marek, R. *J. Phys. Chem. A* **2010**, *114*, 1985−1995.
(37) Maliňáková, K.; Novosadová, L.; Pipíška, M.; Marek, R. *ChemPhysChem* **2011**, *12*, 379−388.
(38) Barone, V.; Cossi, M.; Tomasi, J. *J. Chem. Phys.* **1997**, *107*, 3210−3221.
(39) Cossi, M.; Scalmani, G.; Rega, N.; Barone, V. *J. Chem. Phys.* **2002**, *117*, 43−54.
(40) Flukiger, P.; Portmann, S. *MOLEKEL 4.3*; Swiss Center for Scientific Computing: Switzerland, 2002.
(41) Ramsey, N. F. *Phys. Rev.* **1950**, *78*, 699−703.
(42) Auer, D.; Kaupp, M.; Strohmann, C. *Organometallics* **2004**, *23*, 2347−3655.
(43) Auer, D.; Strohmann, C.; Arbuznikov, A. V.; Kaupp, M. *Organometallics* **2003**, *22*, 2442−2449.
(44) Auer, D.; Kaupp, M.; Strohmann, C. *Organometallics* **2005**, *24*, 633−6337.
(45) Pipek, J.; Mezey, P. G. *J. Chem. Phys.* **1989**, *90*, 4916−4926.
(46) Pipek, J. *Int. J. Quantum Chem.* **1989**, *36*, 487−501.
(47) Kutzelnigg, W.; Fleischer, U.; Schindler, M. In *NMR Basic Principles and Progress*; Diehl, P., Fluck, E., Günther, H., Kosfeld, R., Seelig, J., Eds.; Springer-Verlag: Berlin, 1990; Vol. *23*.
(48) Bühl, M.; Kaupp, M.; Malkina, O. L.; Malkin, V. G. *J. Comput. Chem.* **1999**, *20*, 91−105.
(49) Kaupp, M., Bühl, M., Malkin, V. G., Eds. *Calculation of NMR and EPR Parameters Theory and Application*; Wiley-VCH: Weinheim, 2004.
(50) Vaara, J. *Phys. Chem. Chem. Phys.* **2007**, *9*, 5399−5418.
(51) Buijse, M. A.; Baerends, E. J. *J. Chem. Phys.* **1990**, *93*, 4129−4141.
(52) Li, S.; Chesnut, D. B. *Magn. Reson. Chem.* **1985**, *23*, 625−638.
(53) Li, S.; Chesnut, D. B. *Magn. Reson. Chem.* **1990**, *24*, 93−100.
(54) Bond, D.; Schleyer, P. v. R. *J. Org. Chem.* **1990**, *55*, 1003−1013.
(55) Biekofsky, R. R.; Pomilio, A. B.; Contreras, R. H.; Orendt, A. M.; Facelli, J. C. *J. Phys. Chem.* **1990**, *94*, 7418−7423.